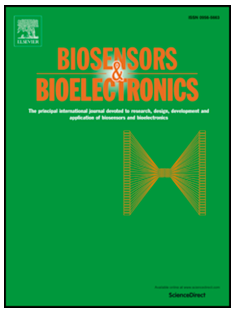

An origami electrical biosensor for multiplexed analyte detection in body fluids

Yu Shen, Sidharth Modha, Hideaki Tsutsui, Ashok Mulchandani

PII: S0956-5663(20)30709-0

DOI: https://doi.org/10.1016/j.bios.2020.112721

Reference: BIOS 112721

To appear in: *Biosensors and Bioelectronics*

Received Date: 20 July 2020

Revised Date: 8 October 2020

Accepted Date: 10 October 2020

Please cite this article as: Shen, Y., Modha, S., Tsutsui, H., Mulchandani, A., An origami electrical biosensor for multiplexed analyte detection in body fluids, *Biosensors and Bioelectronics* (2020), doi: https://doi.org/10.1016/j.bios.2020.112721.

CRediT Author Statement:

Ms. Ref. No.: BIOS-D-20-02471

Yu Shen: Conceptualization, Methodology, Software, Formal Analysis, Investigation, Writing – Original Draft, Writing – Review & Editing, Visualization. **Sidharth Modha**: Investigation, Writing – Review & Editing. **Hideaki Tsutsui**: Conceptualization, Methodology, Resources, Supervision, Funding Acquisition, Funding Acquisition, Writing – Review & Editing. **Ashok Mulchandani**: Conceptualization, Methodology, Resources, Writing – Review & Editing, Supervision, Project Administration, Funding Acquisition, Writing – Review & Editing.

An origami electrical biosensor for multiplexed analyte detection in body fluids

Yu Shen[a], Sidharth Modha[b], Hideaki Tsutsui[b, c, d], Ashok Mulchandani[a, *]

a. Department of Chemical and Environmental Engineering, University of California, Riverside, Riverside, CA 92521, USA.

b. Department of Bioengineering, University of California, Riverside, Riverside, CA 92521, USA.

c. Department of Mechanical Engineering, University of California, Riverside, Riverside, CA 92521, USA.

d. Stem Cell Center, University of California, Riverside, Riverside, CA 92521, USA.

*Corresponding author email address: adani@engr.ucr.edu (Ashok Mulchandani)

Abstract

We developed an affordable, highly sensitive, and specific paper-based microfluidic platform for fast multiplexed detections of important biomarkers in various body fluids, including urine, saliva, serum, and whole blood. The sensor array consisted of five individual sensing channels with various functionalities that only required a micro liter-sized sample, which was equally split into aliquots by the built-in paper microfluidics. We achieved the individual functionalizations of various bioreceptors by employing the use of wax barriers and 'paper bridges' in an easy and low-cost manner. Pyrene carboxylic acid-modified single-walled carbon nanotubes (PCA/SWNTs) were deposited by quantitative inkjet printing with an optimal 3-dimensional semiconductor density on a paper substrate. Multiple antibodies were immobilized onto the SWNTs surface for highly sensitive and specific field-effect transistor (FET)/chemiresistor (CR) biosensors. We explored the optimal sensing conditions for the paper-based CR biosensor to achieve high sensitivities and specificities towards the target biomarker proteins (human serum albumin (HSA) and human immunoglobin G (HIgG)) and achieved an ultralow detectable concentration of HSA and HIgG at 1.5 pM. Besides, origami folding was employed to simplify the fabrication process further. The sensing platform described in this work was cost-effective, semi-automated, and user-friendly. It demonstrated the capability of having multiple sensing functions in one paper-based microfluidic sensing platform. It envisioned the potential of a point-of-care device with full-analysis for practical diagnostics in an ASSURED (Affordable, Sensitive, Specific, User-friendly, Rapid and robust, Equipment-free and Deliverable to end-users) fashion for a quick test of targets of interest.

Keywords

Paper-based microfluidics; inkjet printing; multiplexed detections; single-walled carbon nanotubes; FET/chemiresistive biosensors; ASSURED criteria.

1. Introduction

Many efforts have been made towards developing diagnostic devices that meet the ASSURED criteria of being **a**ffordable, **s**ensitive, **s**pecific, **u**ser-friendly, **r**apid and robust, **e**quipment-free, and **d**eliverable-to-those-who-need-it (Smith et al., 2018). Given that over 95% of the deaths in low-income countries are due to major infectious diseases and cancers, early diagnosis is of great importance to the overall health of human beings (Yager et al., 2006). Point-of-care (POC) diagnostic devices using low-cost substrates and easy fabrication methods are being extensively studied. Paper exhibits great advantages beyond other polymer-based flexible substrate materials (Gao et al., 2017; Vengasandra et al., 2010; Wongkaew et al., 2013; Wu et al., 2015) for being low-cost with intrinsic capillary microfluidics, easily disposable and biocompatible, requiring no external pumps, low-instrumentation and easy-to-assemble. Therefore, paper has become a popular substrate to build ASSURED biosensing platforms (Choi et al., 2016; Fava et al., 2019; Li et al., 2017; Shen et al., 2019).

Paper-based biosensors using colorimetric/chemiluminescence and electrochemical detection with pre-deposited reagents and automated or semi-automated microfluidics that have been widely explored (Cheng et al., 2010; Cinti et al., 2017; Fava et al., 2019; Lamas-Ardisana et al., 2018; Martinez et al., 2007; Sun et al., 2018; Wang et al., 2018). Nevertheless, many colorimetric devices are primarily qualitative, while the ones that are quantitative have a poor limit of detection (LOD) in the micromolar or millimolar ranges (Martinez et al., 2007), require special cameras or scanners to capture the light intensities (Ge et al., 2012), and often necessitate a fixed lighting environment for accurate measurements (Hu et al., 2014). Electrochemical biosensors, on the other hand, require bulky liquid reservoirs for the redox reaction to occur as well as employment of multiple antibodies (capture antibodies and reporter probe antibodies) and labels (enzymes, dyes, nanoparticles, etc.) for complicated sandwich assays (Mettakoonpitak et al., 2016). Current label-based immunoassays are limited by the lack of an ideal label that is compatible with all potential target analytes, the inability to achieve LOD at nanomolar to attomolar levels, and the long assay time. As such, label-free immuno-nanosensors are an active research subject. Compared to the previously developed technologies, the label-free field-effect transistor (FET)/chemiresistor (CR)-based biosensors are more appealing in providing high

sensitivities and selectivities for target biomarkers (Mulchandani and Myung 2011; Tran and Mulchandani 2016).

Owing to their intriguing physical, chemical, and electrical properties, carbon-based nanomaterials have emerged as potential candidates for the development of next-generation miniaturized biosensors (Syedmoradi et al., 2017; Tran and Mulchandani 2016; Yang et al., 2015). Single-walled carbon nanotubes (SWNTs) have been employed extensively as transducer elements in FET/CR sensors due to their high surface-to-volume ratio, which causes the Debye length (λ_D), a measure of electric field penetration into a bulk material, to be comparable to the dimensions of these nanostructures (Tran and Mulchandani 2016). This leads to significant modulations of their electronic properties upon exposure to chemicals, enabling the label-free detection of analytes with higher sensitivities and lower LODs. Moreover, SWNTs FETs/CRs can be integrated with modern microelectronics in multifunctional devices that detect multiple analytes simultaneously (Wan et al., 2011). Thus, SWNTs are the promising semiconducting transducer material to fabricate FET/CR biosensors in this work. Methods to fabricate paper-based microfluidic channels range from sophisticated photolithography to facile printing methods (Xia et al., 2016). However, the high cost of the toxic reagents/solvents of most fabrication methods of paper-based microfluidics still poses a challenge to fabricating a well-defined biosensor array on a porous paper substrate with high sensitivity and specificity to conduct multi-analyte detection with minimal sample requirements. On the other hand, wax printing shows several merits such as 1) a simple fabrication process of printing and baking with adequate pattern resolutions, 2) rapid fabrication in minutes, 3) low cost (easy to obtain paper and wax), 4) environment-friendly (no organic solvents), and 5) ease of disposal after use by incineration (Shen et al., 2019). Hence, wax printing is employed in this work to build the multiplexed paper microfluidic channels in a facile and economic manner.

Herein, we present a new biosensing platform featuring a paper-based microfluidic FET/CR array for highly sensitive and selective multiplexed detections of important biomarkers in body fluids.

2. Methods and experiments

2.1 Inkjet printing fabrication of the paper-based SWNTs CR array

DMP-2831 inkjet printer (FUJIFILM Dimatix, Inc.) was used to print the conductive silver leads (Metalon JS-B25P, NovaCentrix, Inc.) and pyrene carboxylic acid (PCA)-modified SWNTs, from now-on designated as PCA/SWNTs, CRs. Cellulose paper (Whatman Grade 1 chromatography paper, 20 cm squares) was used as the substrate for depositing the sensor arrays. Drop spacing was 20 μm and droplet speed was 6-8 m/s. Wax patterns were designed using GNU Image Manipulation Program (GIMP) software and exported as TIFF files. Xerox ColorQube 8880DN was used to print wax barriers on paper substrate. Details of PCA/SWNTs synthesis, inkjet printing, wax printing and gas sensing for optimization of device resistance is included in **supplementary information**.

2.2 Functionalization of the SWNTs CRs

All functionalization steps were done at room temperature, and all reagents were purchased from Sigma-Aldrich unless noted otherwise. Monoclonal anti-human serum albumin (HSA) and anti-human immunoglobin G (HIgG) antibodies were purchased from Medix Biochemica (6502 SP-2) and Sigma-Aldrich (I6260), respectively. The PCA/SWNTs CRs were submerged in 0.1 M MES buffer (pH 5.5) containing N-(3-Dimethylaminopropyl)-N′-ethylcarbodiimide (EDC) at 5 mM and N-Hydroxysuccinimide (NHS) at 2.5 mM for 20 min, followed by rinsing with phosphate buffer (PB), 10 mM at pH 7.4 unless otherwise specified, and tapped dry. In sequence, 20 μL of 50 μg/mL of each antibody in PB, 10 μL of 0.1 M ethanolamine in PB, and 10 μL of 0.1 wt% Tween-20 in PB were added to each sensing sites and incubated individually at room temperature for 2 h, 15 min, and 30 min, respectively, followed by PB wash and tapped dry the paper surface after each incubation step.

2.3 Device assembly, sample preparation and electrical measurement

From top to bottom, single-sided tape with an inlet hole, paper bridges, sensing layer, absorption layer, and sealing tape were assembled. The assembled devices were stored with full humidity. Priming buffer (10 mM PB, pH 7.4), HSA or HIgG were spiked into various matrices and drop cast at the device inlet. With the source-drain voltage of 0.1 V (e.g., no gate voltage), the electrical resistance changes of the CR arrays were monitored continuously with respect to time

using a Keithley source meter (Model 2636) while full humidity at room temperature was maintained. Detailed description is presented in **supplementary information**.

3. Results and Discussions

3.1 Design of the paper-based microfluidics with the paper bridges

First, we designed the 5-petal shaped hydrophilic channels on paper to equally split one sample into five aliquots for individual sensing channels. As shown in **Figure 1(a)**, one sample injected at the central inlet would split into five. By the capillary force, each aliquot would have traveled along the hydrophilic channel, encountered the CR, and finally reached the waste reservoir at the pattern perimeter. In this design, the CRs can be inkjet-printed in the middle of each channel, followed by incubations with different bioreceptors for 2 hours. However, here came the paradox that, while the capillary force transported the aliquots dispensed at the center to the destination spontaneously, it also allowed unwanted diffusion of various bioreceptors throughout the pattern during the incubations—a critical step to achieving multiplexed sensing functions. **Figure 1(a)** illustrates this unwanted diffusion using dyed solution. To mimic the 2-hour incubation, the dye was added in one channel and was observed to travel into the other four channels and contaminated them with the non-desired molecules. Similarly, the CRs would have been contaminated with the undesired bioreceptors during bioreceptor incubations, which would have resulted in loss of selectivity for all sensing channels. Therefore, it was necessary to keep local functionalizations free of cross-contaminations and maintain the high specificity for each CR biosensor, while taking advantage of the self-wicking capability of paper to transport the sample and wash fluids from the central inlet to sensing channels.

Next, to address this predicament, we employed five pairs of extra wax barriers before, and a structure named ‘paper bridges’ after the bioreceptor incubations. Firstly, to confine the various incubation solutions for the duration (2 hr) of biofunctionalization, extra wax barriers that were perpendicular to the direction of the microfluidic channels were printed simultaneously with the 5-petal pattern (**Figure 1(a)**). The 5-petal channel with extra wax barriers were melted through the thickness of the paper and formed unyielding hydrophobic barriers, thus the sensing channels were partitioned by the extra wax barriers into separated regions where no diffusion was observed, as indicated by the non-interacting dye and clear water regions in **Figure 1(a)**. For the

2-hr span of the incubation, extra wax barriers successfully prevented the cross-contaminations of different bioreceptors and preserved the high specificity of each sensing channel, as discussed in the crosstalk control. Secondly, after the functionalizations, the CR arrays were ready to receive the sample transport. However, the radial hydrophilic channels were now blocked by the extra wax barriers, which prevented the transport of liquid samples. Therefore, we employed the paper bridges to overcome this issue, as shown in **Figure 1(b)** (see **Figure S1** in **supplementary information** for the paper bridge fabrication). The paper bridges acted as hydrophilic bridges for the liquid samples to flow over the extra wax barriers. The full-complement of the paper bridges, which had two concentric rings with melted discontinuous magenta wax, were accomplished by assembling them on top of the extra wax barriers to provide the hydrophilic openings and reconnect the microfluidic channels (see **Figure S2** in **supplementary information** for microfluidic dimensions). The middle image in **Figure 1(b)** shows the dyed equal flows of dye solution in the reconnected channels.

Figure 1(c) shows the mass fabrication process of the sensing platforms. On a 20-cm-squared Whatman Grade 1 paper, silver ink was inkjet-printed, and heat annealed to develop conductive silver leads. Paper is known to be sensitive to heat, but the optimized annealing temperature (200 ˚C) had a negligible impact on the capillary flow in the paper (**Supplementary Information**). Next, the 5-petal pattern with extra wax barriers was printed and melted to form the hydrophobic barriers, followed by bovine serum albumin (BSA) blocking for all channels to prevent non-specific adsorption (**Figure S3** in **supplementary information**). After that, a formulated ink of water-based PCA/SWNTs (Shen et al., 2019) was inkjet printed in the middle of each channel with an optimized inkjet condition to maintain the printing consistency (see **supplementary information** for ink formulation and inkjet printing condition) After the PCA/SWNTs were printed and the formulation solvent evaporated at room temperature, conjugation of the bioreceptors on the SWNTs was performed. To demonstrate the capability of multi-analyte detections of the microfluidic sensing platform, we used two different antibodies: anti-HSA and anti-HIgG. They were individually incubated to produce two sets of CR immunosensors, whereas the fifth CR transducer served as a control (i.e., no antibody conjugated). Thus, the sensing platform was equipped with two sensing replicas for two targets (HSA and HIgG) and one control channel used as a reference for evaluating the background noise. After biofunctionalizations, the absorption pad, sensing layer and paper bridges were assembled and

held in place by tape. Note that the top tape layer tightly sealed any gaps between the sensor array layer and the paper bridges to ensure the connections of hydrophilic paper sections. The adsorbing pad was used as a waste reservoir and provided adequate capillary pumping. As a result, the sensing platform could handle up to ~250 μL of liquid. These changes allowed individual functionalizations of the sensor in each channel and retained the utility of the microfluidic channels to transport fluid toward the sensor and subsequently to the waste pad. Meanwhile, the resistances were recorded for individual CRs by connecting the platform to a source meter at the electrical vias.

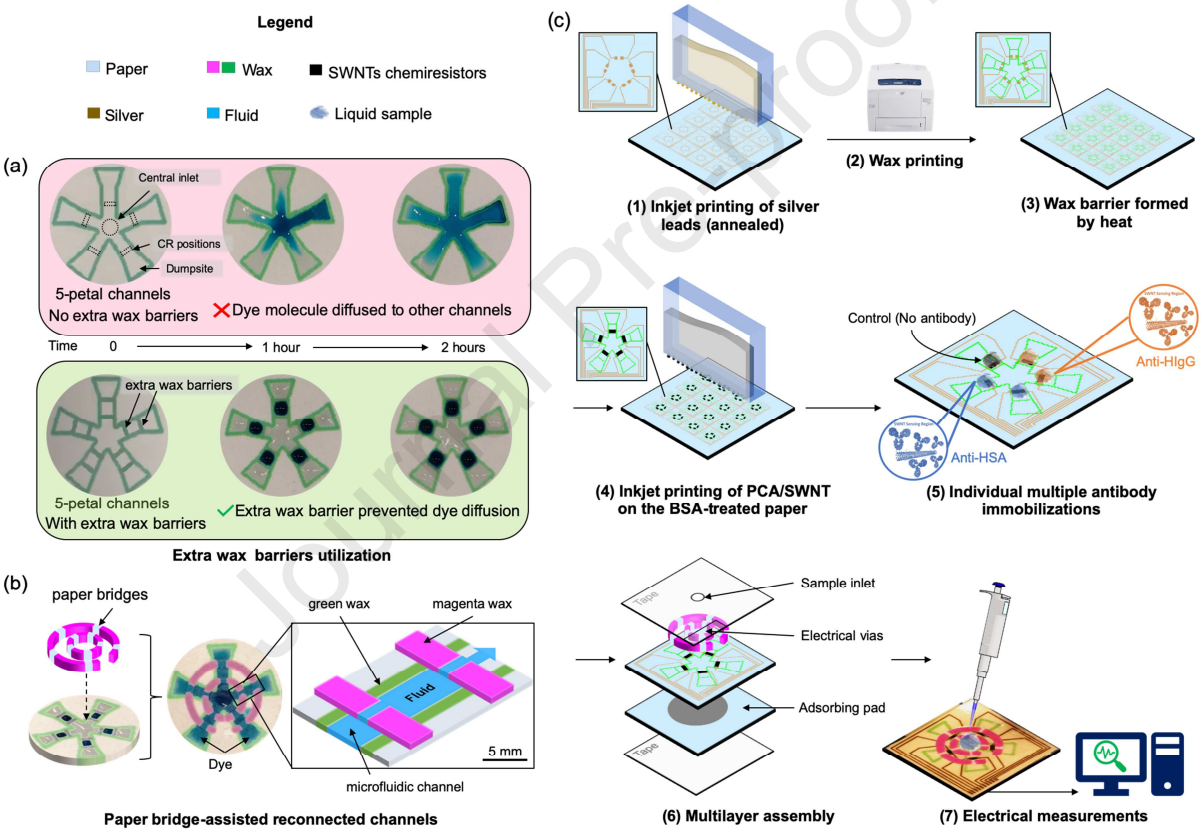

Figure 1. Design of the 5-petal microfluidic channels using extra wax barriers and paper bridges and an overall process flow of the sensor fabrication and testing. (a) Top: Pictures showing the dye spreading to other channels over 2 hr without extra wax barriers. Bottom: Pictures showing the individual incubations of dyes in each sensing channel with the extra wax barriers. (b) The assembly of the paper bridges and the sensor layers. Paper bridges had two concentric rings with melted discontinuous magenta wax to provide hydrophilic bridges for channel reconnections.

Two goals were achieved as 1) individual liquid confinement and 2) paper-based microfluidics reconnection. (c) An overview of the fabrication process: 1) inkjet printing of silver leads, followed by annealing at 200 ˚C for 2 hr; 2) Wax printing of the hydrophobic patterns on the paper; 3) 5 min heating at 170 ˚C to melt the wax into paper substrate; 4) Inkjet printing of PCA/SWNTs ink and drying; 5) Functionalization of multiple antibodies individually; 6) Layer-by-layer assembly of the sensing platform; and 7) measurements of sensor signals.

3.2 Optimization of SWNTs network density

Since SWNTs are rod-shaped nanomaterials and percolate into the paper during the deposition to form a 3-dimensional network (Hu et al., 2004), we varied the SWNTs network density by inkjet-printing different number of layers of the PCA/SWNTs ink. The electron microscopy images of SWNTs network on paper are shown in **Figure S5**. The network density increased with printing more layers and resulted in a percolation profile in **Figure 2(a)**. The percolation profile was plotted with the logarithm of the inverse of the sheet resistance $R_{\square}$ (**supplementary information**) versus the number of printing layers, and can be divided into three regions: (1) non-percolated, (2) linear percolation, and (3) complete percolation. $1/R_{\square}$ increased significantly with increasing printing layers in the non-percolated region, linearly in the linear percolation region, and slowly in the complete percolation region. In the non-percolated region, there could be scant SWNTs to form the electron paths from source to drain electrodes as well as the inadequate affinity binding sites for the sensing activity. On the contrary, in the complete percolation region, there could be too many metallic SWNTs short-circuiting the semiconducting SWNTs, which might conceal the responses due to antigen-antibody affinity binding events near the semi-conducting SWNTs. Therefore, we hypothesized that a network composed of neither too little nor too much semiconducting and metallic SWNTs would be desirable for building a highly sensitive CR and anticipated that the most sensitive density of SWNTs network would be in the linear percolation region with initial resistance from 9.6 ± 0.14 kΩ to 80.5 ± 1.8kΩ (**Figure 2(a)**). To test our hypothesis, we evaluated the PCA/SWNTs CR arrays with various $R_{\square}$ for a gas sensing with NO_2 in N_2 (**Figure S4** in **supplementary information**). All subsequent electrical responses in this work, for both gas and liquid phase sensing, are defined by **Equation**

1, where R_0 is the resistance of the SWNTs CR after priming with N_2 or liquid buffer, and R is the stable resistance after each exposure to the samples. For the NO_2 gas sensing, the Fermi level shifted towards the valence band with NO_2 adsorbed on the p-typed SWNTs and resulted in an increase of conductance (Kong et al., 2000). As shown in **Figure 2(b)**, the ideal initial resistance range of 25 kΩ to 35 kΩ at 25 ˚C and relative humidity (RH) ~ 30% gave the highest sensitivity, which was also confirmed by additional liquid phase biosensing (**Figure S6** in **supplementary information**). Therefore, all subsequent sensors were prepared to have a similar initial resistance value.

$$Response = \frac{R - R_0}{R_0} = \frac{\Delta R}{R_0} \quad \#\boldsymbol{Equation\ 1}$$

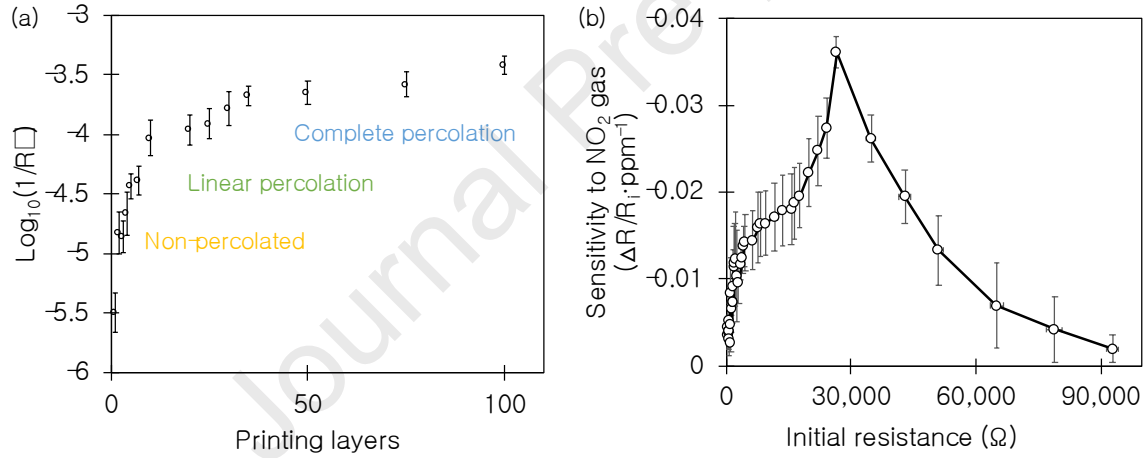

Figure 2. Percolation profile of the inkjet-printed PCA/SWNTs network on the paper substrate and the optimization of the CR initial resistances. (a) The percolation profile of inkjet-printed PCA/SWNTs network on paper substrate. (b) Sensitivities of PCA/SWNTs networks with various initial resistances. Each data point was the average of 5 sensors. All error bars represented the ±1 standard deviation.

3.3 Optimization of the sensing environment and controls

Results in **Figure S7 (see supplementary information)** exemplify that the ambient humidity was unable to stabilize the responses. At first, adsorption of water in 10 mM PB to the dry CR

lead to a considerable increase in the resistance since the water molecules were electron-donating and thus n-doped the p-typed SWNTs (Han et al., 2012). Upon adding a sample of HSA/PB, the resistance increased further, but followed by a steep decrease to near the starting resistance instead of a plateau (**Figure S7**). We attributed this phenomenon to the dynamic equilibrium of water adsorption due to sample additions and desorption due to water evaporation, which was vital to the steady readings of the electrical responses. Thus, to eliminate the impact of evaporation, we implemented a PB priming step to create a locally saturated liquid environment before analyte additions and maintained a full RH during the whole sensing process. With full humidity maintained during storage, SWNTs were eventually counter-doped by n-doping water molecules to be n-typed semiconductors (Han et al., 2012). As a consequence, we observed an additional decrease in resistance in the first 4 minutes, as shown in **Figures 3(a) & (c)**. In this sensing platform, two additions of 20 μL PB made the sensor baseline readings stable and any subsequent changes in resistance were results of affinity binding events instead of the variation of moisture level during the sensing process. Another benefit of priming was to reduce sudden sensor distortion due to paper fiber swelling from the absorption of a water-based liquid sample (Carstens et al., 2017). The target proteins, however, at the sensing pH, were possibly behaving as an electron acceptor and repelled the electron carriers in the semiconducting SWNTs (Ingrosso et al., 2012; Liu et al., 2011; Zhou et al., 2000). Thus, upon the exposure to the negatively charged analyte, the n-type SWNTs CR were exhibiting increases in the resistance.

Positive and negative controls demonstrated the selectivity of the biosensors. The positive control experiments with SWNTs blocked with tween-20 (without antibodies) that were exposed to PB (blank), 15 μM HSA, and 15 μM HIgG produced low responses of 2.17%, 3.28%, and 3.64%, respectively (**Figure S8** in **supplementary information**). This established the effectiveness of tween-20 blocking process in preventing non-specific adsorption of analytes to SWNTs. Similarly, negative control experiments in which biosensors functionalized with anti-HSA and anti-HIgG were exposed to 20 μL of PB (blank) showed significantly smaller responses (< 5%) compared to their targeted analytes (**Figure S9** in **supplementary information**). This corroborated that the high responses were indeed from the antigen-antibody binding.

3.4 Sensitivity and limit of detection

Figure 3 (a) & (c) show dynamic responses of the sensor arrays to each target protein from 0.15 pM to 15 μM in PB. After priming, as new samples (20 μL) of higher concentrations of the target proteins were added (4 μL per channel), the CR resistances increased and reached higher plateaus quickly for higher concentrations. **Figure 3 (b) & (d)** show the calibration plots of plateau responses as a function of antigen concentrations in PB. The sensors responded linearly to both analytes between 1.5 pM to 15 μM, which included the biologically meaningful range for potential urine analysis (Attar et al., 2019; Turner et al., 1970). The sensitivities (slope of the calibrations) were 0.081 per Log_{10} [nM of HSA] and 0.091 per Log_{10} [nM of HIgG]. The lowest detectable concentration for HSA and HIgG in PB estimated by S/N = 3 were 1.5 pM, which was comparable or better than the reported to-date for these proteins in terms of both the linear ranges and detection limits (**Table S1** in **supplementary information**). Furthermore, as evidenced by a low residual standard deviation (RSD) of 11.2% and 12.2% for responses from 6 sensors each of HSA and HIgG at 15 μM, respectively, the sensors had excellent precision. The high sensitivity of SWNTs network FET/CR based biosensors fabricated on non-porous substrates have been well documented and the physics behind it explained in detail (Tran and Mulchandani, 2016). However, the sensitivities observed in this work for the SWNTs network CR on paper substrate are markedly superior. We ascribed the ultrahigh sensitivity of the present paper-based CR arrays to the porous paper substrate that promotes 1) improved connectivity of SWNTs due to firm adhesion of individual SWNTs in porous and rough paper surface compared to uniform surface of Si/SiO_2 or glass solid substrate (Han et al., 2012); and 2) weaker counter-ion screening, consequently higher sensor response, from concave corners that are preferably formed/promoted when SWNTs lie on cellulose fibers compared to flat solid substrate (Shoorideh and Chui 2014). Also contributing to the high sensitivity can be the high loading of antibodies for effective capture of antigens that was the result of large loading of -COOH groups from the attached PCA on SWNTs (Shen et al., 2019).

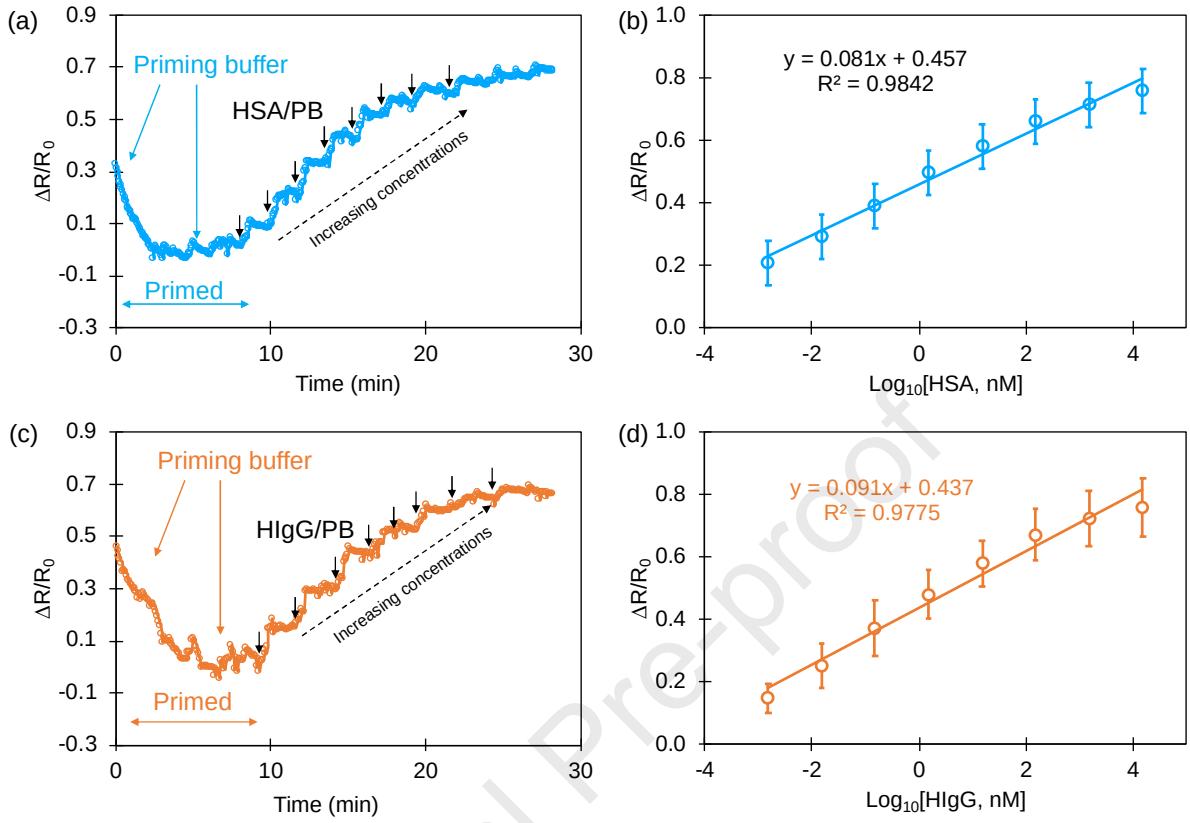

Figure 3. Real-time monitoring of the changes in resistance during the priming process and sensing process for additions of 20 μL samples prepared in PB and their corresponding calibration curves. (a) Real-time monitoring of the sensing process for the detections of HSA/PB (pH 7.4). (b) Calibration curve for the detection of HSA/PB with a linear regression y = 0.081Log_{10}[HSA] + 0.457 with R^2=0.9842. (c) Real-time monitoring of the sensing process for the detections of HIgG/PB (pH 7.4) (d) Calibration curve for the detection of HIgG/PB with a linear regression y = 0.091Log_{10}[HIgG] + 0.437 with R^2=0.9775. Each data point is the average of 6 sensors. All error bars represent ±1 standard deviation.

3.5 Specificity and stability

To test the specificity of the sensing channels, crosstalk controls were examined by checking the electrical responses when the sensor encounters the wrong analyte (i.e., anti-HSA/SWNTs with HIgG/PB and anti-HIgG/SWNTs with HSA/PB). As shown in **Figure 4(a)**, the sensors with the wrong target only resulted in 13.4 % and 11.1 % increase in the electrical responses, respectively,

for anti-HSA/SWNTs sensor with 15 μM HIgG and anti-HIgG/SWNTs with 15 μM HSA, which were minimal compared to the positive sensing responses of 86.2% and 88.8%, respectively, for 15 μM of HIgG/PB and HSA/PB. Therefore, the extra wax barriers successfully prevented cross-contamination of the two antibodies during the functionalization and lead to the high specificities between different sensing channels. However, the crosstalk did give rise to 2- to 3-fold larger responses (10 - 15%) than the other controls (< 5%). We attributed this to the drift of the SWNTs CRs over the ~ 40 min sensing period, and the quality of the commercial antibodies that were not perfectly purified to ensure absolute specificity and thus resulted in higher responses in the crosstalk controls.

Storage stability (i.e., shelf life) is of great significance to maintaining the quality and robustness of the diagnostic devices. Thus, batches of the fully integrated paper-based CR array were prepared and stored for varying durations under full humidity at room temperature or 4 ˚C. Sensors were tested on day 7, 14, and 21. The sensitivities were calculated in the same manner as previously described and were normalized against the sensitivities at day 0. As shown in **Figure 4(b)**, at 4 ˚C the sensors retained nearly 100% sensitivity for three weeks. On the other hand, when stored at room temperature, there was a 11.2% and 22.0% drop in sensitivity after 3-weeks for anti-HSA/SWNTs sensors and anti-HIgG/SWNTs sensors, respectively. These results demonstrated good overall stability of antibodies conjugation and SWNTs transducers.

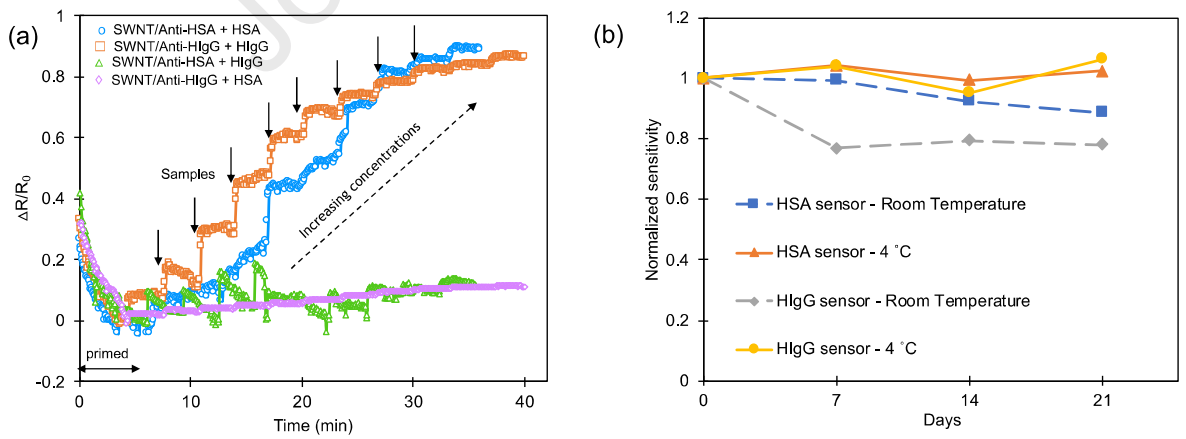

Figure 4. Real-time monitoring of the changes in resistance for sample sensing and controls. (a) Comparison between the responses from HSA and HIgG sensing and the crosstalk control. (b) Normalized sensitivity of the sensor array stored at room temperature or 4˚C.

3.6 Application of sensors to samples in biological matrices

Detection of proteins as disease biomarkers in body fluids is routinely performed in healthcare. To demonstrate the potential of the described paper-based CR biosensor arrays, we applied the sensors to detect HSA and HIgG in human body fluids such as urine, saliva, serum and whole blood. We used an artificial urine (AU) matrix to simulate the real-life sensing environment (Brooks and Keevil 1997). Since the AU contained a lot of salts and had high ionic strength, which minimized the Debye length, PB washes were necessary to recover the responses of the responses of SWNTs CR from the affinity binding of antigen-antibody interaction. After PB priming, 20 μL AU spiked with the target proteins were added to individual sensors. As shown in **Figures 5(a) & (b)**, the responses for both targets were reduced compared to the PB samples due to the high ionic strength of the AU matrix at about 1.18 M, resulting in small Debye length (Chu et al., 2017; Kaisti 2017; Shoorideh and Chui 2014). After the first wash passing through the CRs, some responses were recovered, and the second and third wash recovered the responses further, reaching steady levels comparable to those in PB samples. The possible mechanism was that the washes diluted the local AU matrix and removed the salts to the absorbing pad, making a local environment with low ionic strength close to 24 mM (the ionic strength of PB), and a larger Debye length to overturn the charge screening and recover the responses (Kaisti 2017). The insets in **Figure 5(a) & (b)** show that detection of HSA and HIgG in AU after implementing 3 washings of 30 μL each were in excellent agreement with the responses in PB, indicating the minimal matrix effects left after the washing with PB.

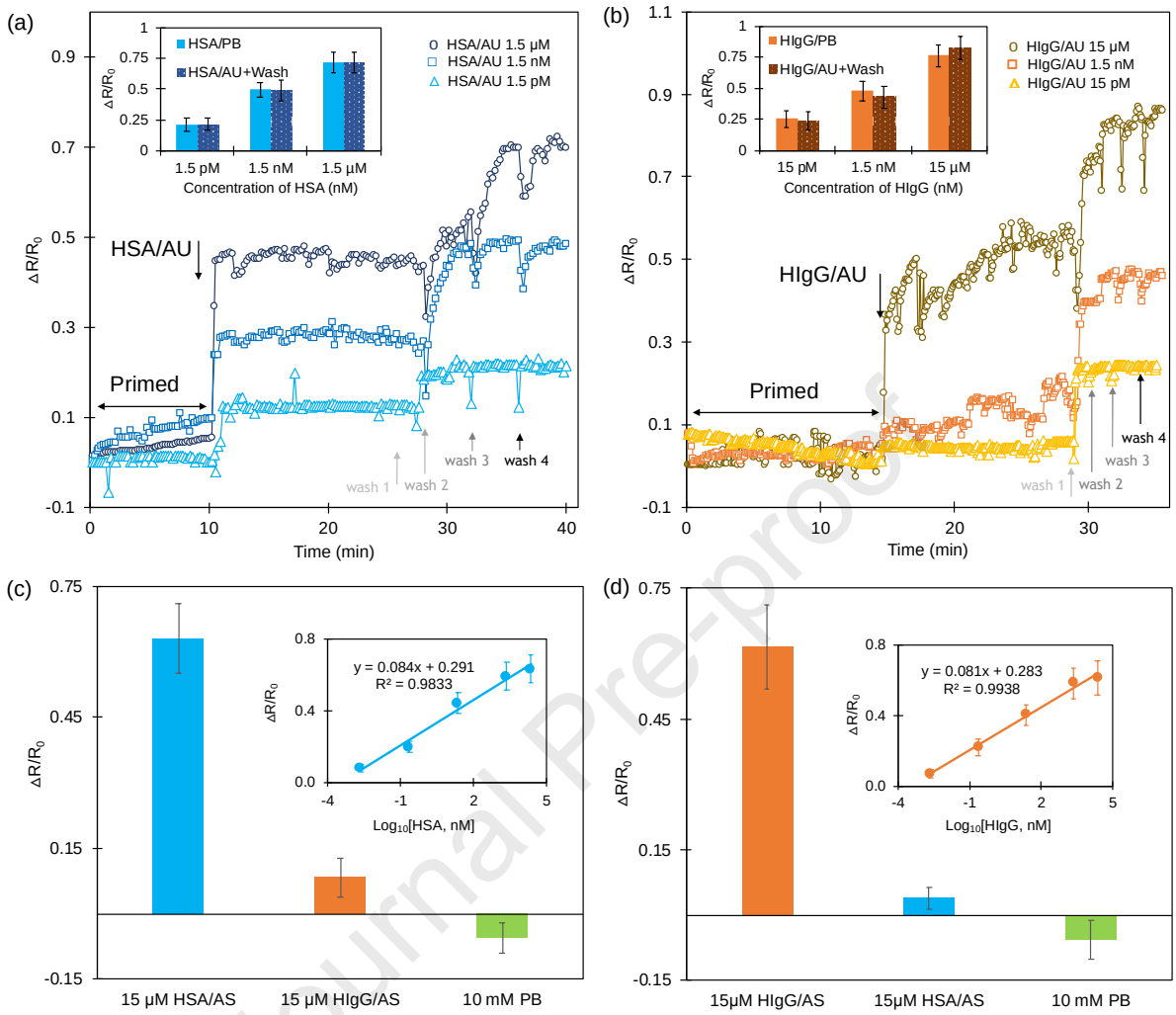

Figure 5. Sensing responses from samples (20 µL) in complex matrices. Real-time monitoring of the detection of (a) HSA and (b) HIgG spiked in an AU matrix (pH 7.4) with full humidity at room temperature. 30 μL of each 10 mM PB wash diluted the local matrix and recovered the electrical responses. Comparison of responses from (c) anti-HSA functionalized sensors and (d) anti-HIgG functionalized sensors to 15 µM HSA and 15 µM HIgG spiked in an AS sample after washing with 10 mM PB and controls. Inset figures show comparison of responses for (a) HSA and (b) HIgG in AU after washing and PB, calibration plots of (c) anti-HSA functionalized sensors for HSA and (d) anti-HIgG functionalized sensors for HIgG detection in AS after washing. Each data point is the average of 6 sensors. All error bars represent ±1 standard deviation.

Saliva is a non-invasively collected body fluid sample and contains many important biomarkers (Khan et al., 2019; Tlili et al., 2010). To administer a test of biomarkers in a salivary matrix, we spiked HSA and HIgG into the artificial saliva (AS) to simulate the salivary matrix (Tlili et al., 2010). A similar sensing protocol with PB washes for the AU sample was employed. Although the mucin in AS matrix increased fluid viscosity, there was no obvious discrepancy of the flow rate and fluid delivery time to those of PB and AU samples. As shown in **Figures 5(c) & (d)**, controls exhibited minimal responses compared to the detection of salivary HSA and HIgG, which gave linear regression of $y = 0.084\text{Log}_{10}[\text{HSA, nM}] + 0.291$ with $R^2 = 0.9833$, and $y = 0.081\text{Log}_{10}[\text{HIgG, nM}] + 0.283$ with $R^2 = 0.9938$, respectively. With the washing steps, the sensitivities (slopes) to salivary HSA and HIgG were 100.12% and 88.67% to those in PB, respectively.

Furthermore, we tested the sensors with human serum and whole human blood from commercial sources (collected from healthy donors). As the concentrations of the target proteins in serum and blood largely exceeded the dynamic range of the sensor array, serum and blood were analyzed after diluting 10^7 times with PB. Column 3 in **Table S2 (**see **supplementary information)** reports the concentrations of HSA and HIgG found in these diluted samples using the calibration plots in **Figure 3(b) & (d)** (for detailed calculations please see **Table S3** in **supplementary information)**. Subsequently, we spiked the diluted samples with known concentrations of HSA and HIgG (**Table S2** column 4), analyzed with the same sensor arrays and determined the percent recovery (**Table S2**, last column). As shown in the table, the recoveries (i.e. agreement) ranged from 90% to 108% (average of 96.75±7.8%). These high recoveries, i.e. accuracy of the sensors, was achieved without buffer washes since the serum and blood were diluted 10 million-fold in PB thus diluting the concentration of salts and also minimizing the non-specific adsorption from blood cells and other proteins. These results showed the wide applicability of the integration of the SWNTs-based chemiresistive biosensors with the paper-based microfluidics to both simple PB and complex matrices of artificial urine, saliva, human serum, and human blood.

3.7 Origami devices with easy assembly

Despite the easy assembly required, the critical alignment of the hydrophilic pathways and the secure adhesion between the tapes and layers are vital for the paper-based microfluidic transport. Misalignment between paper-sections and the lack of solid lamination can lead to unequal sample splitting and thereby unreliable electrical signals and inaccurate results. The use of origami techniques to make 3D devices from a single paper sheet as an alternative to stacking multiple layers has been reported (Arduini et al., 2019; Ding et al., 2016). Therefore, to further standardize the fabrication and reduce hand assembly errors, we designed a wax-patterned origami device that demonstrated the same idea of employing extra wax barriers and paper bridges (**Figure 6(a)**). The origami was composed of three layers: 1) top layer for sample-splitting and paper-bridging, 2) middle layer with CR biosensor arrays for multiplexed detections and 3) bottom layer with sufficient absorbing capability. Unlike the manually assembled ones, origami devices benefited from the precise trimming by CO_2 laser cutting that helped facile alignment of the three layers thereby reducing the human labor and error (**Figure 6(b)** and **supplementary video**). **Figure 6(c)** shows that the dynamic responses for PB priming and sensing of the target proteins in the origami device were comparable to the previous layer-by-layer assembled paper-based microfluidic label-free CR biosensing arrays. The primed CRs exhibited large increases in resistance upon addition of target analytes and low responses in the blank control. The origami devices provided a cost-effective and practical method to integrate both the well-controlled paper-based microfluidics and highly sensitive and selective chemiresistive biosensor array into one for label-free multiplexed detection of important biomarkers.

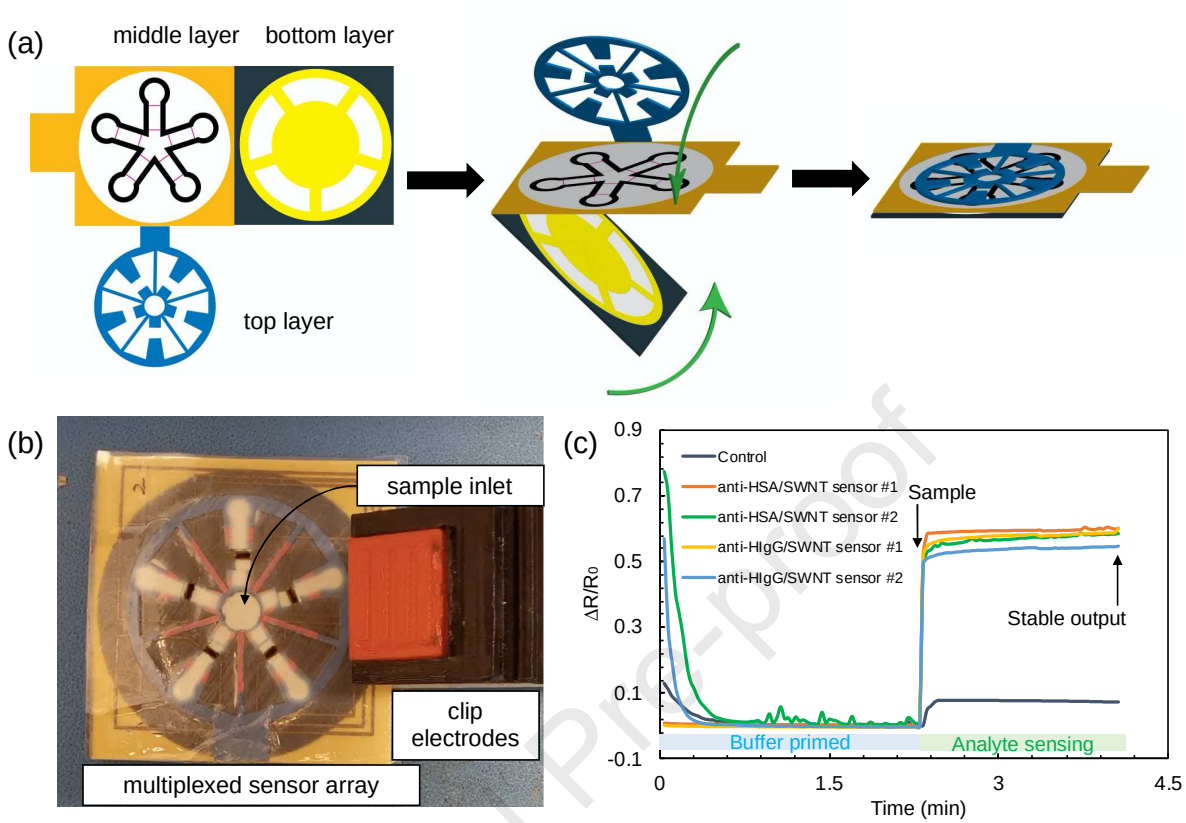

Figure 6. Fabrication and sensing protocol of the origami device. (a) Assembly of the three-layered origami device. (b) Image of the origami device with clip electrodes attached. (c) The processed electrical output of the origami device.

4. Conclusions

We developed an affordable and practical paper-based sensing platform for rapid multiplexed label-free detections of relevant biomarkers by employing antibody conjugated SWNTs CRs with the top-down integration of paper-bridging microfluidics. With the use of extra wax barriers and paper bridges, the fully assembled devices, both manual and origami assembled, successfully split one sample into equal aliquots and transferred into individual sensing channels with negligible crosstalk. With optimal percolation density of the inkjet-printed SWNTs network, we immobilized anti-HSA and anti-HIgG antibodies on multiple CRs for a demonstration of detections of multiple biomarkers in a single microliter-size sample. The device showed high sensitivity, specificity and stability for the detection of the target analytes. In complex sample

matrices including artificial urine and saliva, and diluted human serum and blood, efficient buffer washes successfully bypassed the reduction in signals due to shortened Debye length in highly ionic or viscous solutions. Furthermore, precise and undemanding origami design was employed to achieve simple fabrications of the biosensor array towards mature and practical assembly of the described diagnostic device. The reported biosensing platform is expected to promote the future development and adoption of FET/CRs on paper substrates in not only the resource-limited diagnostic applications such as ASSURED devices, but also other sensing scenarios, including but not limited to, on-site environmental monitoring, rapid detection of pathogens, and quick examinations of forensic samples.

Acknowledgements

This work is supported by National Science Foundation Grant 1606181 and National Institute of Justice Award 2019-NE-BX-0006. AM acknowledges W. Ruel Johnson Chair in Environmental Engineering.

References

Arduini, F., Cinti, S., Caratelli, V., Amendola, L., Palleschi, G., Moscone, D., 2019. Biosensors and Bioelectronics 126, 346-354.

Attar, A.M., Richardson, M.B., Speciale, G., Majumdar, S., Dyer, R.P., Sanders, E.C., Penner, R.M., Weiss, G.A., 2019. ACS applied materials & interfaces 11(5), 4757-4765.

Brooks, T., Keevil, C., 1997. Letters in applied microbiology 24(3), 203-206.

Carstens, F., Gamelas, J.A., Schabel, S., 2017. Cellulose 24(1), 295-309.

Cheng, C.M., Martinez, A.W., Gong, J., Mace, C.R., Phillips, S.T., Carrilho, E., Mirica, K.A., Whitesides, G.M., 2010. Angewandte Chemie International Edition 49(28), 4771-4774.

Choi, J.R., Hu, J., Tang, R., Gong, Y., Feng, S., Ren, H., Wen, T., Li, X., Abas, W.A.B.W., Pingguan-Murphy, B., 2016. Lab on a Chip 16(3), 611-621.

Chu, C.-H., Sarangadharan, I., Regmi, A., Chen, Y.-W., Hsu, C.-P., Chang, W.-H., Lee, G.-Y., Chyi, J.-I., Chen, C.-C., Shiesh, S.-C., 2017. Scientific reports 7(1), 5256.

Cinti, S., Minotti, C., Moscone, D., Palleschi, G., Arduini, F., 2017. Biosensors and Bioelectronics 93, 46-51.

Ding, J., Li, B., Chen, L., Qin, W., 2016. Angewandte Chemie International Edition 55(42), 13033-13037.

Fava, E.L., Silva, T.A., do Prado, T.M., de Moraes, F.C., Faria, R.C., Fatibello-Filho, O., 2019. Talanta 203, 280-286.

Gao, Y., Ota, H., Schaler, E.W., Chen, K., Zhao, A., Gao, W., Fahad, H.M., Leng, Y., Zheng, A., Xiong, F., 2017. Advanced Materials 29(39), 1701985.

Ge, L., Wang, S., Song, X., Ge, S., Yu, J., 2012. Lab on a Chip 12(17), 3150-3158.

Han, J.-W., Kim, B., Li, J., Meyyappan, M., 2012. The Journal of Physical Chemistry C 116(41), 22094-22097.

Hu, J., Wang, S., Wang, L., Li, F., Pingguan-Murphy, B., Lu, T.J., Xu, F., 2014. Biosensors and Bioelectronics 54, 585-597.

Hu, L., Hecht, D., Grüner, G., 2004. Nano letters 4(12), 2513-2517.

Ingrosso, C., Bianco, G.V., Lopalco, P., Tamborra, M., Curri, M.L., Corcelli, A., Bruno, G., Agostiano, A., Siciliano, P., Striccoli, M., 2012. Nanoscale 4(20), 6434-6441.

Kaisti, M., 2017. Biosensors and Bioelectronics 98, 437-448.

Khan, M.S., Dighe, K., Wang, Z., Srivastava, I., Schwartz-Duval, A.S., Misra, S.K., Pan, D., 2019. Analyst 144(4), 1448-1457.

Kong, J., Franklin, N.R., Zhou, C., Chapline, M.G., Peng, S., Cho, K., Dai, H., 2000. science 287(5453), 622-625.

Lamas-Ardisana, P., Martínez-Paredes, G., Añorga, L., Grande, H., 2018. Biosensors and Bioelectronics 109, 8-12.

Li, B., Zhang, Z., Qi, J., Zhou, N., Qin, S., Choo, J., Chen, L., 2017. ACS sensors 2(2), 243-250.

Liu, H., Liu, Y., Zhu, D., 2011. Journal of materials chemistry 21(10), 3335-3345.

Martinez, A.W., Phillips, S.T., Butte, M.J., Whitesides, G.M., 2007. Angewandte Chemie International Edition 46(8), 1318-1320.

Mettakoonpitak, J., Boehle, K., Nantaphol, S., Teengam, P., Adkins, J.A., Srisa-Art, M., Henry, C.S., 2016. Electroanalysis 28(7), 1420-1436.

Mulchandani, A., Myung, N.V., 2011. Current opinion in biotechnology 22(4), 502-508.

Shen, Y., Tran, T.-T., Modha, S., Tsutsui, H., Mulchandani, A., 2019. Biosensors and Bioelectronics 130, 367-373.

Shoorideh, K., Chui, C.O., 2014. Proceedings of the National Academy of Sciences 111(14), 5111-5116.

Smith, S., Korvink, J.G., Mager, D., Land, K., 2018. RSC advances 8(59), 34012-34034.

Sun, X., Li, B., Tian, C., Yu, F., Zhou, N., Zhan, Y., Chen, L., 2018. Analytica chimica acta 1007, 33-39.

Syedmoradi, L., Daneshpour, M., Alvandipour, M., Gomez, F.A., Hajghassem, H., Omidfar, K., 2017. Biosensors and Bioelectronics 87, 373-387.

Tlili, C., Cella, L.N., Myung, N.V., Shetty, V., Mulchandani, A., 2010. Analyst 135(10), 2637-2642.

Tran, T.-T., Mulchandani, A., 2016. TrAC Trends in Analytical Chemistry 79, 222-232.

Turner, M., Johansson, S., Barratt, T., Bennich, H., 1970. International Archives of Allergy and Immunology 37(4), 409-417.

Vengasandra, S., Cai, Y., Grewell, D., Shinar, J., Shinar, R., 2010. Lab on a Chip 10(8), 1051-1056.

Wan, Y., Deng, W., Su, Y., Zhu, X., Peng, C., Hu, H., Peng, H., Song, S., Fan, C., 2011. Biosensors and Bioelectronics 30(1), 93-99.

Wang, Y., Luo, J., Liu, J., Li, X., Kong, Z., Jin, H., Cai, X., 2018. Biosensors and Bioelectronics 107, 47-53.

Wongkaew, N., He, P., Kurth, V., Surareungchai, W., Baeumner, A.J., 2013. Analytical and bioanalytical chemistry 405(18), 5965-5974.

Wu, J., Wang, R., Yu, H., Li, G., Xu, K., Tien, N.C., Roberts, R.C., Li, D., 2015. Lab on a Chip 15(3), 690-695.

Xia, Y., Si, J., Li, Z., 2016. Biosensors and Bioelectronics 77, 774-789.

Yager, P., Edwards, T., Fu, E., Helton, K., Nelson, K., Tam, M.R., Weigl, B.H., 2006. Nature 442(7101), 412.

Yang, N., Chen, X., Ren, T., Zhang, P., Yang, D., 2015. Sensors and Actuators B: Chemical 207, 690-715.

Zhou, C., Kong, J., Yenilmez, E., Dai, H., 2000. Science 290(5496), 1552-1555.

An origami electrical biosensor for multiplexed analyte detection in body fluids

Yu Shen[a], Sidharth Modha[b], Hideaki Tsutsui[b, c, d], Ashok Mulchandani[a, *]

a. Department of Chemical and Environmental Engineering, University of California, Riverside, Riverside, CA 92521, USA.

b. Department of Bioengineering, University of California, Riverside, Riverside, CA 92521, USA.

c. Department of Mechanical Engineering, University of California, Riverside, Riverside, CA 92521, USA.

d. Stem Cell Center, University of California, Riverside, Riverside, CA 92521, USA.

*Corresponding author email address: adani@engr.ucr.edu (Ashok Mulchandani)

Highlights

- Paper microfluidic SWNTs biosensor for ultrasensitive multiplexed detection.
- Wax barriers and paper bridges ensure local functionalization and sample transport.
- Inkjet printing offers precise, fast and low-cost sensor fabrication.
- Patterned printing and origami design simplify sensor fabrication.
- High specificities and reproducibility plus good storage stability.

Declaration of interests

☒ The authors declare that they have no known competing financial interests or personal relationships that could have appeared to influence the work reported in this paper.

☐The authors declare the following financial interests/personal relationships which may be considered as potential competing interests: